Progress In Electromagnetics Research C, Vol. 82, 237–249, 2018

Enhanced HF RFID Detection Area of Mobile Small Tag via Distributed Diameter Coil Resonator

Marjorie Grzeskowiak[1, *], Antoine Diet[2], Megdouda Benamara[1], Christophe Conessa[2], Stephane Protat[1], Marc Biancheri-Astier[2], Francisco de Oliviera Alves[2], Yann Le Bihan[2], and Gaelle Lissorgues[1]

Abstract—To improve HF detection of small RFID tags, a Distributed Diameter Coil (DDC) resonator is included in the reader coil. The key ideas of detection improvement are twofold: using a resonator with Magnetic Resonant Coupling (MRC) and modifying the distribution of diameter and current for each loop of the DDC resonator. These factors allow the magnetic coupling to increase between the reader and the smaller tag, especially in our case where the effective area of the tag is below 0.1% of the reader coil surface. Numerical simulations are carried out using HFSS to confirm the enhancement of the mutual coupling between the tag and the reader coil: the coupling coefficient is used in double-loop coupling (the case of the coupling of two loops), when a third loop (resonator) is inserted. The optimization of the magnetic coupling between a large reader and a small tag with resonator could be realized in changing first the sub-coil diameters, and then the sub-coil number of turns. One figure of merit to quantify the ability of surface detection is defined. A 15% improvement of detection surface in Horizontal Mode is measured at 1 cm of the reader plane in comparison with a conventional coil. Experimental detection measurements on real structures are described to validate statements.

1. INTRODUCTION

This paper focuses on the traceability of small objects, thanks to radiowaves (i.e., thanks to Radio Frequency Identification, RFID) without using any battery and with the advantage of being detected inside a wide detection area (volume of control) whatever the tags orientation. Traceability of small objects with passive RFID tags is a challenge that needs to transfer data and to power wirelessly and efficiently [1]. Whenever the prospecting surface or volume is large, and the tagged object is small, moved and oriented randomly, we have to realize an efficient link. We can cite for instance applications such as a patient moving in a large room [2], surgeon devices inserted in a box on a movable tray or sliding in an inclined tube [3], or tagged pebbles when the reader is moved onto the beach [4]. RFID systems can be classified into two categories: far-field radiation for RF and microwave systems and near-field magnetic induction for LF and HF bands [5]. Far field radiation allows long range but suffers from attenuation in dissipative media while near-field magnetic induction is less sensitive to the dielectric media variation, but provides short range. There are in fact two types of near-field magnetic induction: IC (Inductive Coupling) and MRC (Magnetic Resonant Coupling). MRC [6] provides longer range and larger TX and RX size than IC with higher efficiency [3, 7–9].

We focus, herein, in the detection of RFID tags by magnetic coupling at 13.56 MHz (HF). The technical challenge of our study is due to the size of the RFID tags which are very small compared to the size of the RFID reader coil, that is a non-classical case of study in such RFID, NFC (Near Field

Received 7 February 2018, Accepted 24 March 2018, Scheduled 5 April 2018
* Corresponding author: Marjorie Grzeskowiak (marjorie.grzeskowiak@univ-mlv.fr).
[1] ESYCOM EA 2552, UPEM, ESIEE-Paris, CNAM, 77454 Marne-la-Vallée, France. [2] GeePs UMR 8507, Univ. Paris-Saclay, 91192 Gif Sur Yvette, France.

Communication) nor WPT (Wireless Power Transfer) domains. Additionally, the orientation of the tag is unknown and can be projected into the two orthonormal orientations (or "mode" of detection), i.e., vertical (VM) and horizontal (HM).

Our system is basically composed by an RFID reader, as the TX part, and the RFID tags, as the RXs part. To improve the detection, we propose to study the physical link created by the TX coil (or RFID reader coil) and one RX coil (a tag coil). The results presented in that paper are the optimization of the magnetic coupling and, consequently, the improvement of the detection ability of the system. To improve the efficiency of the physical link in the above-described case and for misaligned TX-RX [9–13], several possibilities can be combined:

1) The use of MR-WPT (Magnetic Resonance Wireless Power Transfer).
2) The optimization of the any coil geometry in the structure [10, 14].
3) The modification of the magnitude and/or the phase of the current per coil. For instance, by active control mechanism on the phase of a crossed dipole coils, as in [12] where transmitting crossed dipole coil with an orthogonal phase difference provides freedom position of the small receiving crossed dipole coil.
4) By coils coverage; for instance, in [11] and with array of coupled resonators in [13], coverage improvements are performed to transfer energy at a specific receiving coil position with a planar array of coupled resonator (relay) coil.

The principle of our study is shown in Fig. 1. As can be noticed, we use resonator in case B and case C, inserted into the surface of the reader coil (TX), to modify the distribution of the magnetic field, because the coupling is too weak in the reference case A. In WPT, powering systems with strong coupling factors use this type of solution by tuning wide resonator, often larger than the TX and RX coils, and are optimized for a single RX, at a single optimum position and orientation. In our case, the coupling coefficient is weak, and we have to reconsider the geometry of the resonator because the goal is to create several areas where the detection, i.e., the coupling, can be improved whatever the orientation and position of the tags (RXs).

The first objective, as identified in this study, is to define an optimum resonator to increase both the detection range and the detection area for a small tag on a specific zone. The addition of a small resonator coil [10], included in the surface of the reader coil, allows the magnetic field generated by the

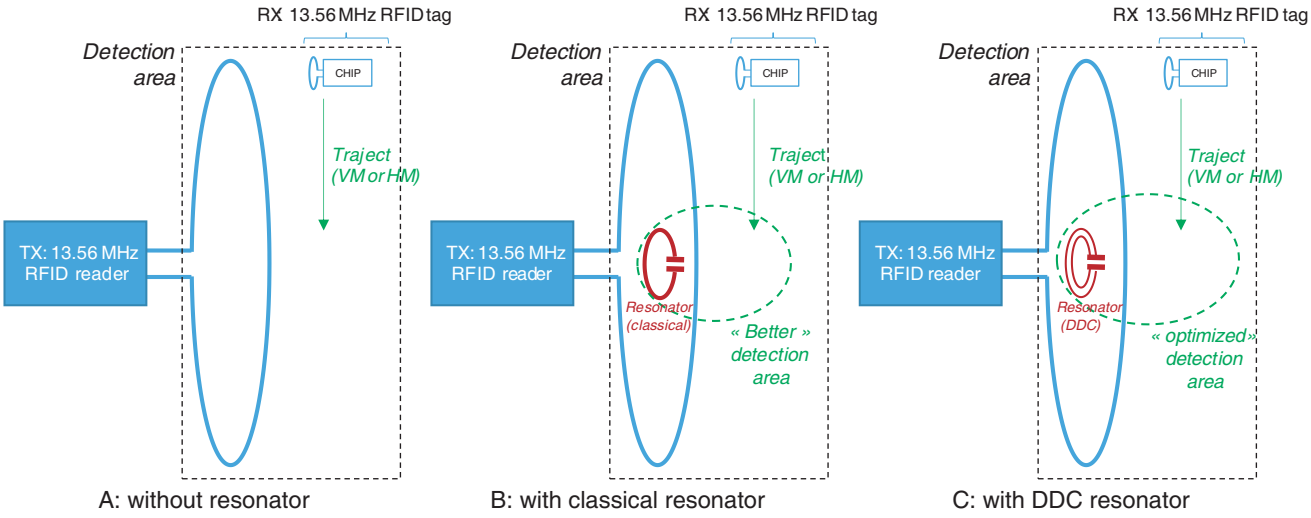

Figure 1. Principle schematic of the study: the goal is to create and optimize some detection areas thanks to resonators. This solution is investigated because the wanted detection area (due to the TX RFID reader coil, in black) is very large compared to the size of the tag effective area (RX RFID tag coil). The use of DDC resonator is a potential optimization in this case of detection, in which the coupling coefficient is low, as it is not the usual case in WPT.

reader to be concentrated; the current distribution of the DDC (Distributed Diameter Coil) coils allows not only the modification of the spatial repartition of the magnetic field but also its vector distribution. This increases the mutual coupling in the best and worst cases which are, respectively, (i) when the tags surface is parallel to this of the DDC surface (HM mode) and (ii) when the tags surface and this of the DDC surface is perpendicular (VM mode).

In this paper, maximization of the power delivered by the reader coil has been done thanks to parametric study by adjusting the diameter of sub-coils and the current per sub-coils of the resonator. DDC (Distributed Diameter Coil) resonator maintains the efficient coupling in 3D spatial variation (distance and location) above its surface in comparison with a conventional coil. The advantages of coplanar coupled resonator in a coil [15] are combined with the optimization of the distribution of each coil of the resonator [16] to improve the RFID detection for a small tag (in comparison with the size of the reader coil).

In the following section, DDC resonator is inserted in the center of a reader rectangular coil [15] whose size determines the detection area. The coupling coefficient between the reader coil (including DDC resonator) and a small tag coil is shown to be increased. The DDC resonators are realized in connecting sub-coils of different radii. In order to optimize the magnetic coupling in a volume, i.e., for several distances, the number of turns for each sub-coil of a given DDC structure is modified in keeping in the same order the inductance of the DDC resonator coil. The equivalent coupling coefficient k_{eq} is calculated between the tag coil and the reader coil (including the resonator). The equivalent coupling coefficient k_{eq} is reported versus the lateral misalignment for both tag coil orientations in horizontal and vertical position/mode (referred to as HM and VM) between the tag coil and the equivalent reader coil. RFID detection tests are compared in a fourth part to evaluate the variation of the RFID detection versus each DDC structure by illustrating detection cartographies. The analysis discussion on the DDC resonator position on the rectangular coil and on the perspectives of this work will conclude our study.

2. EQUIVALENT COUPLING COEFFICIENT VERSUS COPLANAR RESONATOR RADII

Figure 1(a) shows the reader and tag systems. The reader part consists of a rectangular coil and a DDC coplanar circular coil, and the tag part of a small circular coil. As seen in the experimental setup bench, coplanar DDC coil is inserted in the center of a rectangular coil (Fig. 2(b)): its radius r_1 is varied to observe the impact on the inductive coupling with a small coaxial tag coil. The photography (Fig. 2(b)) shows HM and VM modes between the DDC resonator and the tag coils. An equivalent electrical model (Fig. 2(c)) with detail of the calculation of the equivalent impedance Z_{11eq} is obtained [15] and used to calculate the inductive coupling.

The inductive coupling is carried out using HFSS (High Frequency Structure Simulator) which is a commercial full wave software based on the Finite Element Method [17]. For no radiative study it is suggested to add PML boundary condition on the faces of the calculus box. To reduce calculus time, the box is reduced up to 600 times the wavelength and the convergence criteria are chosen by default that causes fluctuations for the simulated results. These fluctuations are up to 4% and are provided by numerical errors. There is a compromise between the meshing of the geometry size to obtain an acceptable level of the errors and the needed fast computer (large hard disk and RAM, intensive processors) to solve problems.

The inductive coupling depends on the equivalent coupling coefficient k_{eq} between the tag coil (1-turn loop of 1 cm diameter) and the equivalent reader coil, where Z_{11eq} corresponds to the equivalent reader impedance composed of the rectangular coil loaded by the coplanar coil, Z_{22} to the self-inductance of the tag coil, and Z_{12eq} to the trans-impedance between the equivalent reader coil and the tag coil. The resonator modifies by the inductive coupling both the reader impedance and the tag impedance. In the case of RFID detection, its impact on the reader input impedance is measured; in our case, for weak coupling, the objective is to increase the magnetic coupling between the reader and the tag in order to improve the RFID detection sensitivity.

$$k_{eq}=\frac{|Z_{12eq}|}{\sqrt{|Z_{11eq}|\times|Z_{22}|}} \tag{1}$$

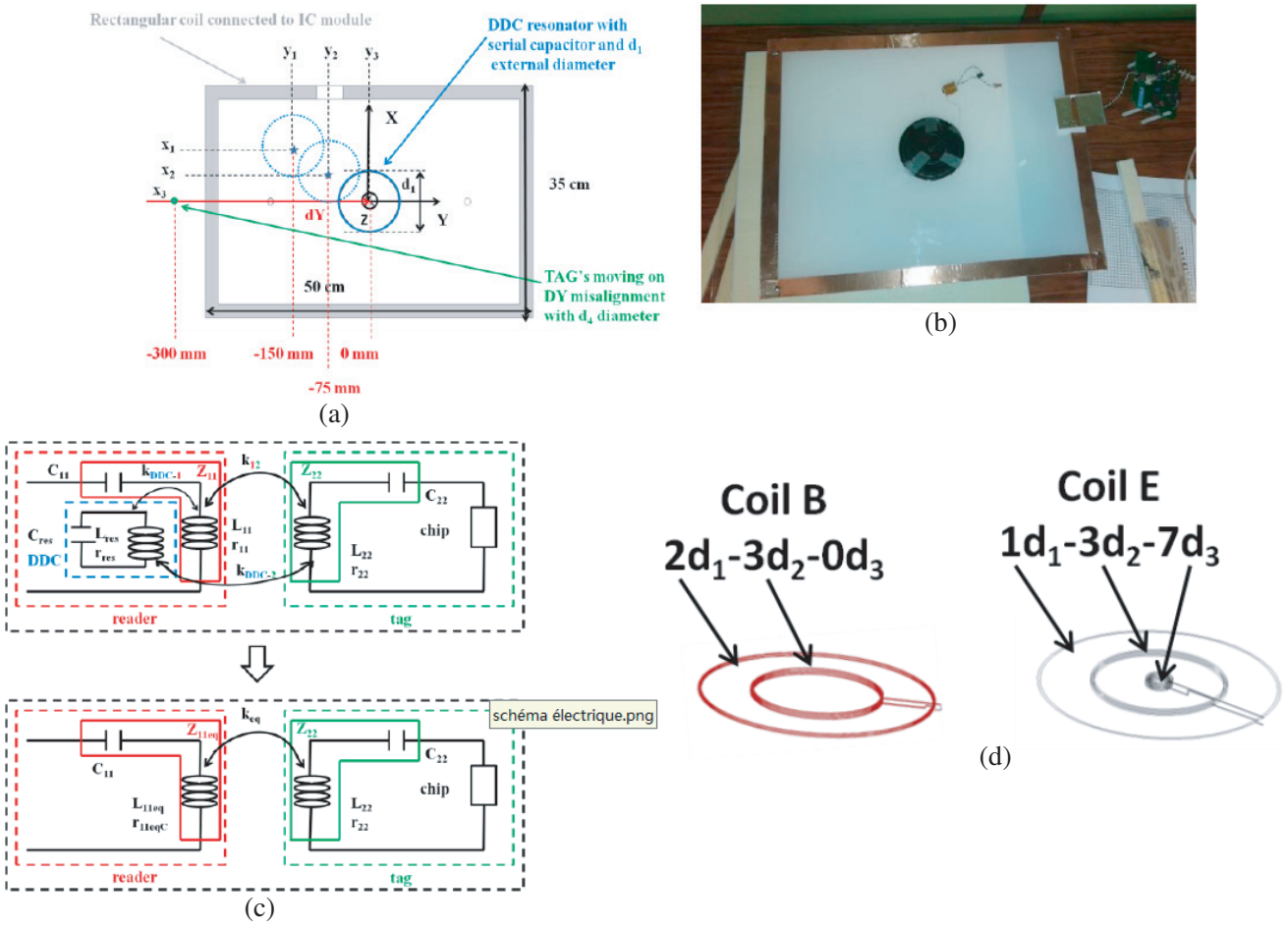

Figure 2. Simulated design of the coils, (a) with the DY misalignment of the tag coil and with variation of the DDC resonator position, (b) reader coil including DDC resonator with matching circuit, (c) equivalent electrical model for the inductive link including DDC resonator in the reader and (d) design of DDC resonators.

The imaginary parts of the complex impedance considered in Equation (1) take into account the inductive phenomenon without capacitor in this parametric part. PEC (Perfect Electrically Conductor) boundaries on strip of 1 µm width replace the metallized wire of the coil without thickness and without substrate to reduce the time process. The simulated coupling coefficient is reported versus the DDC coil radius for several distances between the coaxial coils: the magnetic coupling is optimized versus the DDC radius in Horizontal Mode.

The radius r_1 of the coplanar coil varies from 2 mm to 50 mm when the misaligned distance from the center axis of the resonator is varied from 2 mm to 20 mm (Fig. 3). As expected, higher the misaligned distance, weaker the level of the coupling coefficient [18]. Although, the radius r_1 of the coplanar coil can be increased to maximize the coupling coefficient k_{eq} (1) when the misaligned distance increases. The coupling coefficient presents an optimum radius for each coaxial distance. Sub-coils of different radii could be used to maximize the inductive coupling for different coaxial distances.

In order to observe the inductive coupling above the surface of the DDC coplanar coil with the small tag coil and to take into account the symmetry of the structure, the study can be simplified and the tag coil varied from 0 mm to 50 mm on the DY axis (with 2 mm step and 10 mm coaxial distance). The equivalent coupling coefficient k_{eq} in Eq. (1) is plotted according to the DY misalignment in HM mode (respectively in VM mode) in Fig. 4(a) (respectively in Fig. 4(b)) for DDC radius of 4.5 mm, 25 mm and 45 mm. We can observe peaks of simulated k_{eq} between the 1-turn tag coil and the reader coil (rectangular coil + DDC resonator).

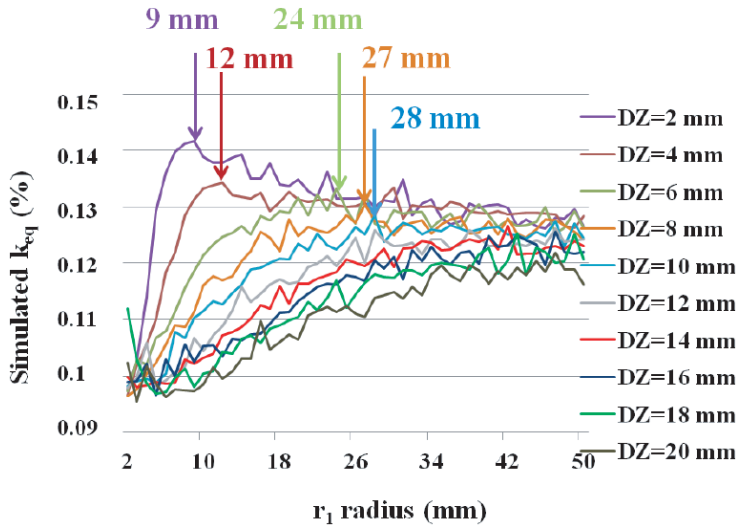

Figure 3. Simulated equivalent coupling coefficient versus the sub-coils radius and the coaxial distance at 13.56 MHz.

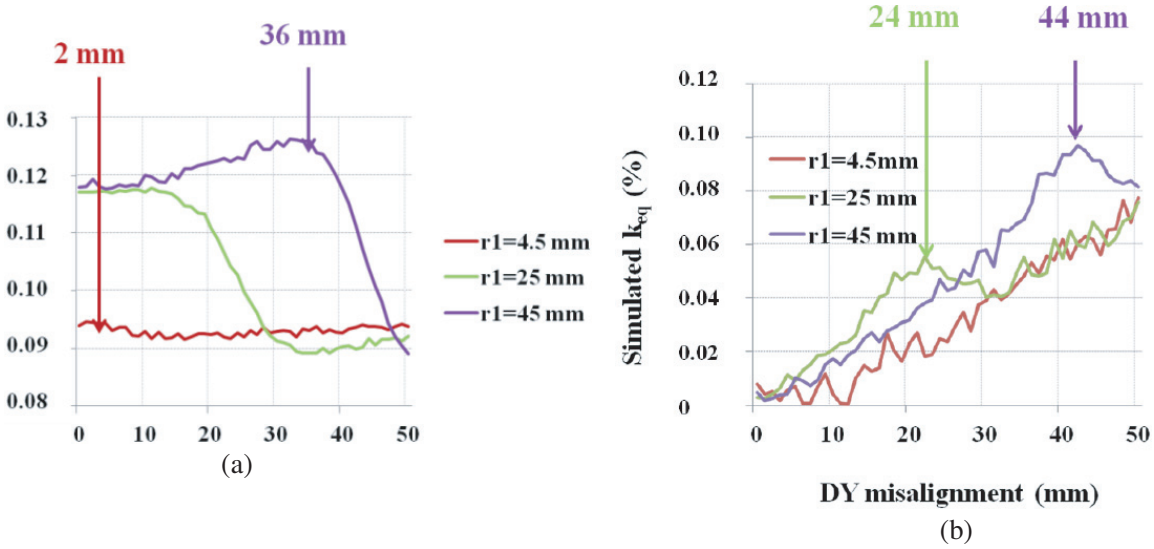

Figure 4. Simulated coupling coefficient versus DY misalignment when the coplanar coil is at the center with radii $r1$ [4.5 mm; 25 mm; 45 mm] at $dz = 10$ mm and 13.56 MHz. (a) In HM mode and (b) in VM mode.

Figure 4 shows the simulated k_{eq} according to the increase of misaligned distance from the center axis of the DDC resonator. The maximum k_{eq} appears at the center of the DDC coil for $R = 25$ mm and at 36 mm of misaligned distance for $R = 45$ mm in HM mode. For VM mode, the maxima appear, respectively, at 24 mm and at 44 mm for radius of 25 mm and 45 mm, corresponding to the surface above the wire. Despite the weakest value in the case of a 4.5 mm radius, the level may have to be increased if the turn number per radius would have been modified, especially in HM mode. The area coverage and range distance can be enhanced in HM and VM modes.

In this part, the interest of using different radii for multi-coils structure has been observed, firstly to increase the level of coupling coefficient at a given point, and secondly to increase the coverage area onto the surface of the coplanar coil. Another degree of freedom can be added in varying the magnitude of current for each radius of the multi-coil structure. This can be done by increasing the turn number for each radius in the resonator. In the following part, this turn number of each radius of DDC coplanar coil

is modified and the impact on the coupling coefficient though a Figure of Merit allows the improvement to be quantified.

3. SIMULATED AND MEASURED COUPLING COEFFICIENT VERSUS DDC STRUCTURE

In this part, we compare three types of DDC resonator, based on modified distribution of the current on each radius of the DDC coplanar coil: a classical single-diameter coil (coil A) and two distributed 3-diameters coils (coils B and E). In simulation, each DDC resonator is inserted in a 50 cm × 35 cm area: the surface of the reader coil is at least 1750 times wider than this of the tag coil ($< 1\,\text{cm}^2$); the ratio is around 20 with an intermediate resonator whose surface corresponds to an area inferior to $20\,\text{cm}^2$. The shape of the reader coil is rectangular to observe potential dissymmetry on the RFID cartography. In order to evaluate the performance of the DDC resonator, we assume that the self inductances of the different coils are identical. Each DDC resonator is designed to present an equal inductance of around 3 µH, and is tuned at the 13.56 MHz resonant frequency with a parallel capacitor C_{res}. The quality factors are equalized by means of parallel resistance R_{res}, as a fix criterion for performance comparison. The radii r_1, r_2 and r_3 are respectively set at 4.5 cm, 2.5 cm and 0.45 cm: ($3d_1$-$0d_2$-$0d_3$) coil, with each number being the number of turns of the associated diameter, corresponds to the conventional coil in [16]. B ($2d_1$-$3d_2$-$0d_3$), and E ($1d_1$-$3d_2$-$7d_3$) are the coils giving the best detection cells in HM and VM modes in [16].

The equivalent reader coils are named A_{reader}, B_{reader}, and E_{reader} coils in connection with each DDC resonator [16]. The rectangular coil is fed in simulation by 1 W power with a 50 Ω lumped port.

In our measurements, each DDC structure is created by enrolling, on a 3D-printed support, an enameled copper wire of 0.022 cm diameter, with enamel thickness between 5 to 50 µm. The spiral small coil is made by double-sided micro-etching (strip of 90 µm, inter-turns of 110 µm and 21 turns for a 1 cm external diameter) on a FR4 substrate. The rectangular reader coil is fabricated with strip of 2.5 cm on 2 mm thickness of plexiglass. The three coils (rectangular coil, DDC resonator and small coil) inputs are connected to Rohde & Schwarz ZVB8 Vector Network Analyser 4 ports with SMA Cable for 27 dBm input power in the [12 MHz–16 MHz] frequency band and 20 kHz frequency step (Fig. 2(b)).

The small tag coil is moved in HM mode (respectively in VM mode) at 10 mm above the reader coil along the DY axis from 0 mm to 50 mm and the equivalent coupling coefficient k_{eq} is reported in Fig. 4(a). The step is smaller in simulation (2 mm) in comparison with this in measurement (10 mm). Due to the difference of the tag coil in simulation (1-turn loop) and measurement (20 turn-loop), the value of its self-inductance is respectively equal to 0.0313 µH and 3.6 µH.

A figure of merit called Coupling Capability of coupling coefficient (CC_k) is proposed in Eq. (2) by means of the integral of $|k_{eq}(y)|$ absolute value along the dY axis. This Figure of Merit (FoM) quantifies the enhancement of the range area while the peak value of the coupling coefficient is in connection with the improvement of the detection range.

$$CC_k = \int_{Y_1}^{Y_2} |k_{eq}(y)|\, dy \tag{2}$$

The observation of the curves profile and the value of the FoM confirms the optimal efficiency of the B_{reader} coil, in simulation and in measurements, in HM mode (Fig. 5(a)), even if the measured k_{eq} and FoM values are weaker in measurements. This can probably be due to the difference of tag coil structures and its connection with the experimental setup with a coaxial cable that disrupts the electromagnetic field.

We have analyzed and demonstrated experimentally that using B_{reader} improves the simulated and measured coupling coefficient between the reader coil and the tag coil in HM mode.

In order to show the distribution of the magnetic field when modifying the number of turns, the simulations with HFSS are performed under the previous values. According to Figs. 6(a)–(c) showing the magnetic field on the z plane, the magnetic fields around the rectangular coil are also identically distributed and very high. It is clear that the magnetic field in the vicinity of the DDC resonator wire is different for each structure. Compared with the conventional coil (Fig. 6(a)) the modification of

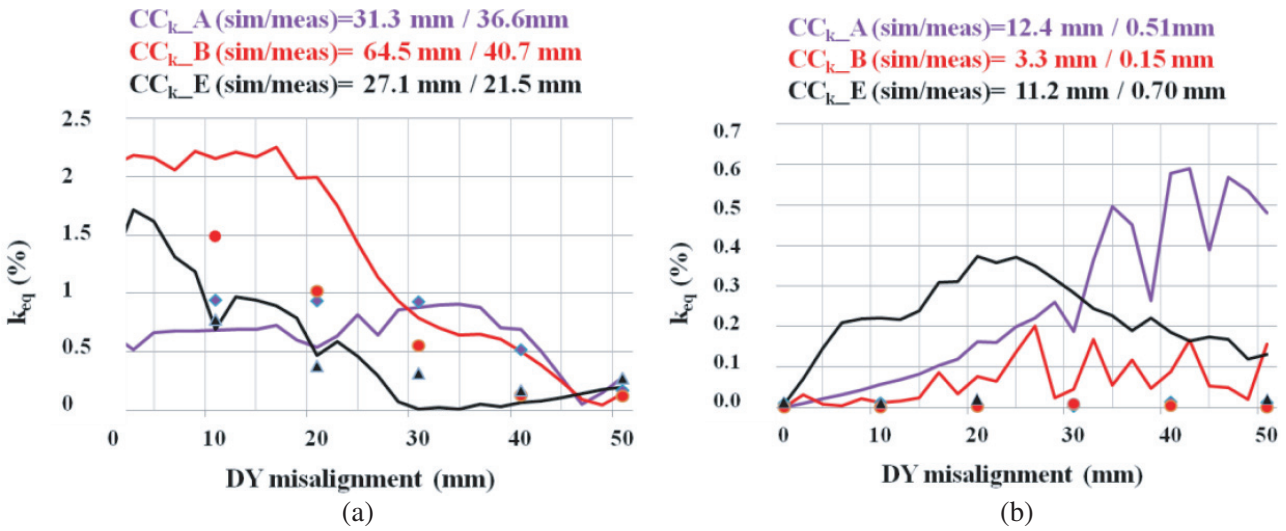

Figure 5. Simulated (solid line) and measured (dot) coupling coefficient versus DY misalignment for $d = 10\,\text{mm}$ at 13.56 MHz. (a) For HM mode, (b) for VM mode.

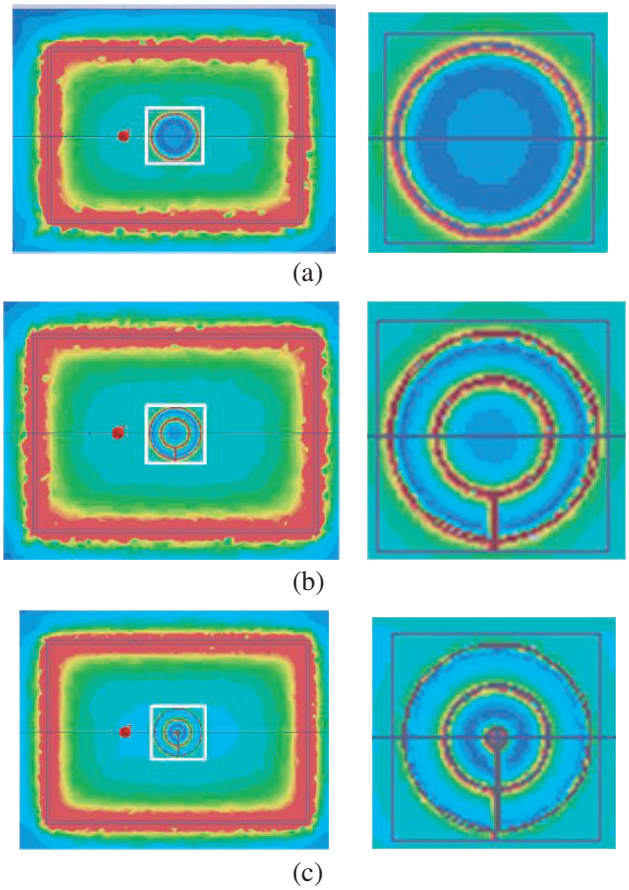

Figure 6. H-field relative magnitude and distribution in $(Y0Z)$ plane with same color scale, in left side, onto the reader coil and in right side, above the resonator. (a) A_{reader}, (b) B_{reader}, (c) E_{reader}.

the resonator diameter and current leads to an enhancement of the magnetic field in the center of the resonators (Figs. 6(b)–(c)) and hence to have more efficient power transmission above the resonators.

The B_{reader}, in HM mode, appears to be the coil that improves the coupling coefficient, while this one stays weak and lower than the other ones in VM mode, in simulation and in measurements. RFID detection range and area coverage are observed in the next section, versus DDC resonator with 0.7 cm diameter tag [19].

4. RFID DETECTION TESTS WITH A SMALL TAG

The detection measurements have been realized with IC module of SIL-2125 reader [20] to validate the improvement of the equivalent coupling coefficient for the B_{reader}. The rectangular coil of 50 cm width and 35 cm length, in which DDC resonator is inserted, is fed by the RFID bench setup. The equivalent reader coil can be matched around 50 Ω by capacitive matching circuit. The variation of inductance values, which supposedly remains constant by empirical formulas [16], is less than 10% in measurement (Table 2) and up to 30% in simulation (Table 1). The intrinsic quality factor depends on the inductance value; consequently, the intrinsic quality factor for each DDC resonator is discrepant for the simulation (Table 1). For this reason, the quality factors have to be equalized with a parallel resistive load to consider each DDC resonator as equivalent electrical resonator and to compare their effect on the tag detection. The discrepancies for the loaded quality factor are less than 1% in simulation and up to 18% in measurement.

Table 1. Electrical characteristics of the simulated DDC coils.

DDC	A	B	E
L_{res} (μH)	2.15	2.46	1.94
R_1 (Ω)	1.89	1.4	1.77
$Q_1 = \frac{L_{res}\omega}{R_1}$	97	150	94
C_{res} (pF)	63	69	70
R_2 (Ω)	8000	6500	7500
$Q_{\text{res}} = \frac{f_r}{\Delta F}$	30.97	30.79	30.86

Table 2. Electrical characteristics of each measured DDC resonator at 13.56 MHz.

DDC	A-DDC	B-DDC	E-DDC
Q_{res}	28	29	33
L_{res} (μH)	3.83	3.53	3.5

The transponder is realized by a two faces spiral coil soldered with the SL2002 ICODE SLI-X IC from NXP which is a HF RFID chip [21]. The detection range is reported in Table 3 when the DDC resonator and the tag are in the center of the reader in HM mode and confirms the detection range enhancement due to the B_{reader} structure. The detection range in the center of the DDCs is increased from 4.5 cm with A_{reader} to a maximum of 5.3 cm with B_{reader} and confirms the link with the improvement of the measured equivalent coupling coefficient.

Table 3. Measured detection range with co-axial tag in HM mode.

DDC resonator	A_{reader}	B_{reader}	E_{reader}
Detection range $(\text{cm})_s$	4.5	5.3	3.9

The small tag of 0.7 cm is moved above the quarter of the reader coil corresponding to 961 cases of 1 cm^2 surface cases. We make the comparison in 4 scenarii: the first scenario is realized without resonator; in the second one, the resonator is in the center (x_3, y_3) as studied previously, and in the third and fourth ones the resonator is tested near the corner (x_1, y_1) and in an intermediate position (x_2, y_2). The detection cartographies are realized at 3 cm height above the quarter of the rectangular

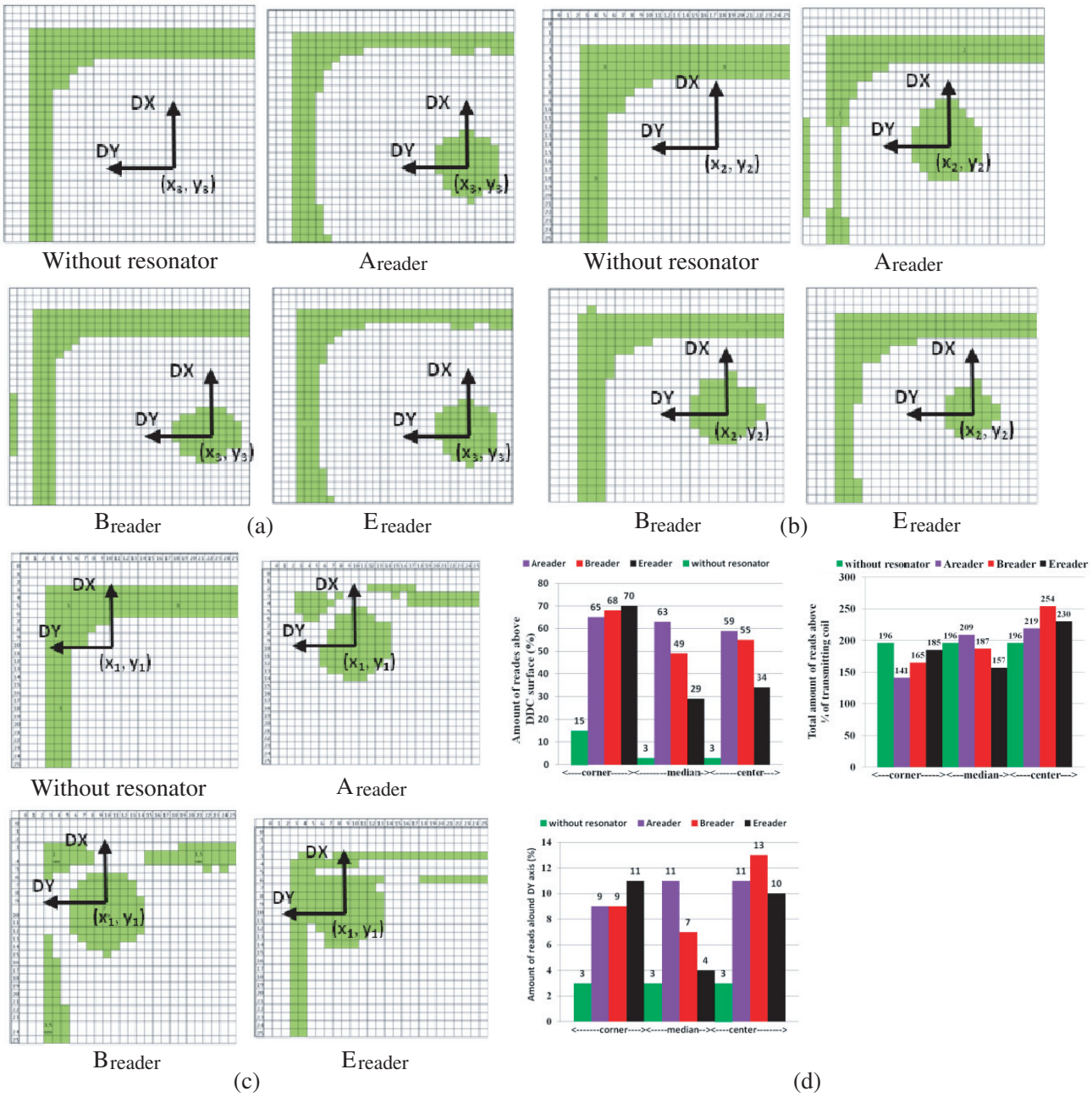

Figure 7. Results of RFID tag detection in VM, for coil A_{reader}, B_{reader} and E_{reader} (colored cells), in function of DX and DY (lateral misalignments) versus the DDC position (corner, median, center) at 30 mm coaxial distance and 13.56 MHz. (a) DDC in the center position ($x_3 = 0$, $y_3 = 0$) in Fig. 2(c). (b) DDC in the median position ($x_2 = -7.5$ cm, $y_2 = -3.75$ cm) in Fig. 2(c). (c) DDC in the corner position ($x_1 = -15$ cm, $y_1 = -7.5$ cm) in Fig. 2(c). d) Results of RFID tag detection cases above DDC surface, above a quarter of the reader surface, and along the y axis.

coil in the top and left surfaces. The circular tag coil of 0.7 cm is placed inside and at the center of each case of 1 cm^2; its surface corresponds to this one of the grid on Figs. 6 and 7. Detection case corresponds to 1 cm^2 surface where the tag is detected.

4.1. RFID Detection in HM for Different DDC Structures

If we compare the scenarii, B_{reader} improves by 15% the surface of detection in comparison with a conventional coil A_{reader}, by 10% with the E_{reader} and up to 30% with the rectangular coil without resonator. For the number of detection cases along the y-axis, B_{reader} is the better structure (an enhancement of 18% with a conventional coil A_{reader} and of 30% with the E_{reader}), while A_{reader} seems

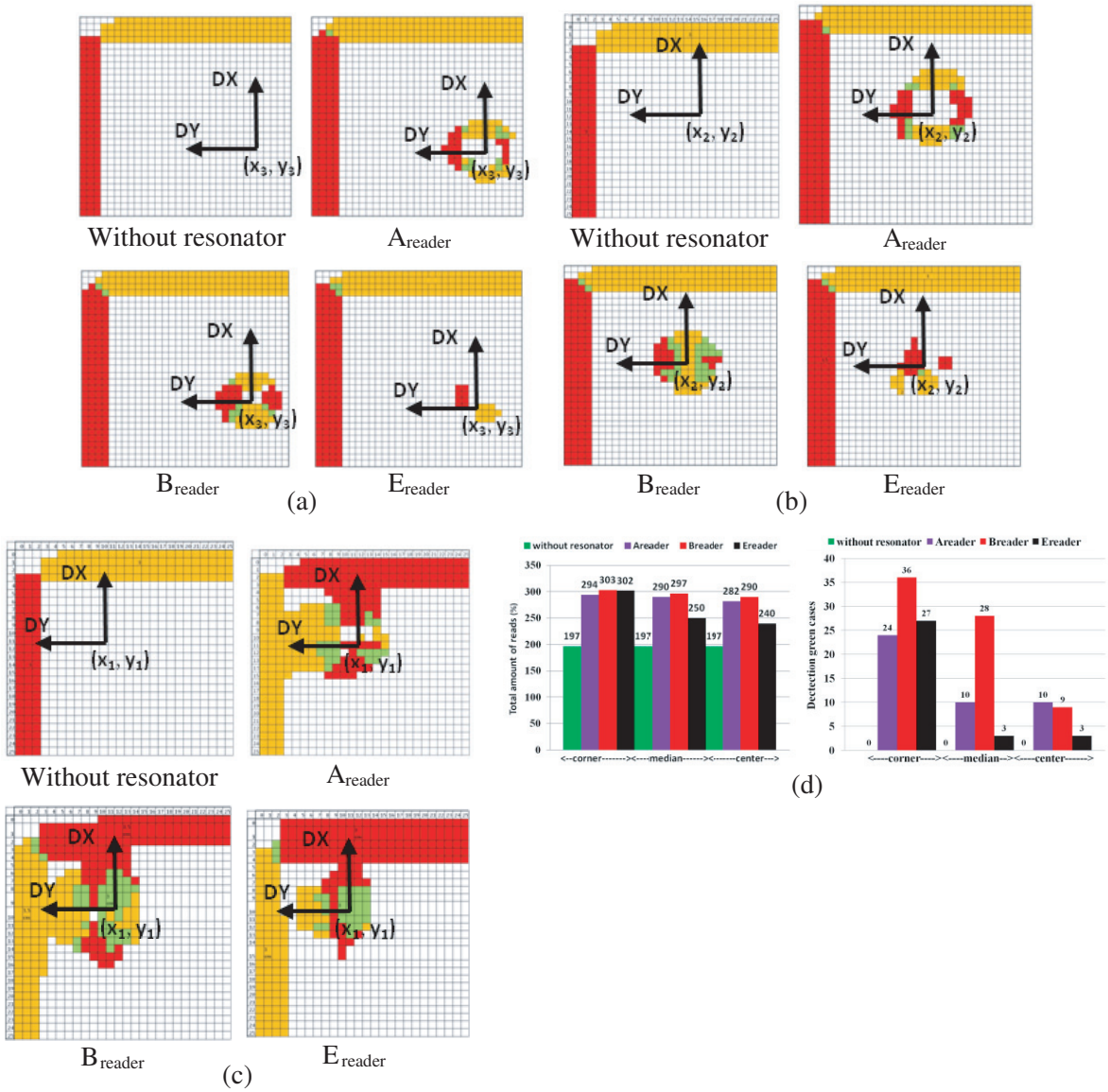

Figure 8. Results of RFID tag detection in VM, for coil A_{reader}, B_{reader} and E_{reader} (colored cells), in function of DX and DY (lateral misalignments) versus the DDC position (corner, median, center) at 30 mm coaxial distance and 13.56 MHz. (a) DDC in the center position ($x_3 = 0$, $y_3 = 0$) in Fig. 2(c). (b) DDC in the median position ($x_2 = -7.5$ cm, $y_2 = -3.75$ cm) in Fig. 2(c). (c) DDC in the corner position ($x_1 = -15$ cm, $y_1 = -7.5$ cm) in Fig. 2(c). (d) Results of RFID tag detection cases whatever its angular rotation.

more efficient in considering the number of detection cases above the DDC surface (an improvement of 7% in comparison with B_{reader} and of 75% with E_{reader}).

The shape of detection area above the DDC is not symmetrical, considering that the distance from the edge is equal to 13 cm on x-axis and 20.5 cm on y-axis. The shape is stretching to the nearest edge.

We report in Fig. 7(d) the number of times that the tag is detected with the structure without resonator (case A in Fig. 1), and A_{reader}, B_{reader} or E_{reader} resonator, called total amount of reads, above DDC surface, above a quarter of the reader coil and along DY axis. It is the total amount of reads: we can see clearly than, when the tag has the previous variation, the best structure for HM detection performances depends on the position of the DDC resonator (Fig. 2(c)) and the B_{reader} isn't the best structure each times (Figs. 7(a) and (d)): near the corner, E_{reader} seems better because of its weak coupling with the rectangular coil (Figs. 7(c) and (d)), and in the median position, A_{reader} will be preferred (Figs. 7(b) and (d)).

Blind zones on RFID cartographies appear when the DDC is in the corner for the A_{reader} and the B_{reader}, because of the stronger coupling between the rectangular coil and the DDC coil: -21.2 or -21.3 dB in comparison with the value of -25 dB for E_{reader}. To minimize the disturbance near the border of the rectangular coil, the quality factor could be reduced. Another solution is to neglect the detection on the borders to maximize the detection inside a surface.

The next part reports the cartographies for VM mode for the 4 previous scenarios.

4.2. RFID Detection in VM for Different DDC Structures

In Fig. 8, the green color corresponds to tag detection whatever its rotation angle, the red one when the tag is in the $(y0z)$ plane and the orange one when it is in the $(x0z)$ plane.

Figure 8(d) shows that B_{reader} outperforms A_{reader} and E_{reader} in terms of the number of detection cases for all three scenarii with resonator.

Due to its current distribution, the B_{reader} may present less sensitivity than other parameters that can impact the RFID detection, such as the frequency shift or the frequency bandwidth to transfer data. In the next part, a discussion on the frequency parameters is ensued, such as about shift and bandwidth of Z_{12eq} trans-impedance between the equivalent reader coil and the tag coil.

4.3. Analysis of the Results versus the Frequency Bandwidth

In order to analyze the frequency impact on the coupling in VM mode for DDC in center, simulated dB_{20} ($magZ_{12}$) is plotted for [12.5 MHz; 14.5 MHz] frequency band and versus the [0; 50 mm] DY misalignment above DDC resonator with the same scale of colormap on Fig. 9.

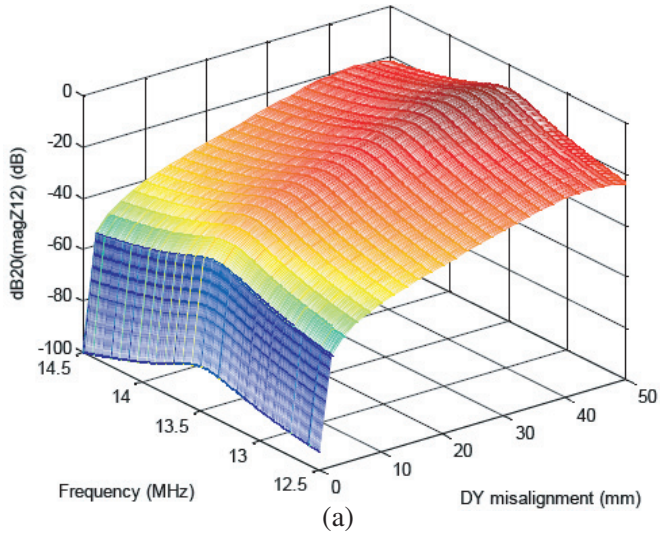

(a)

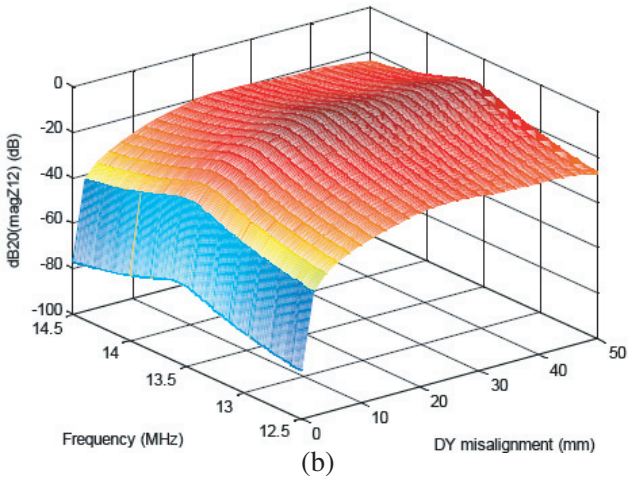

(b)

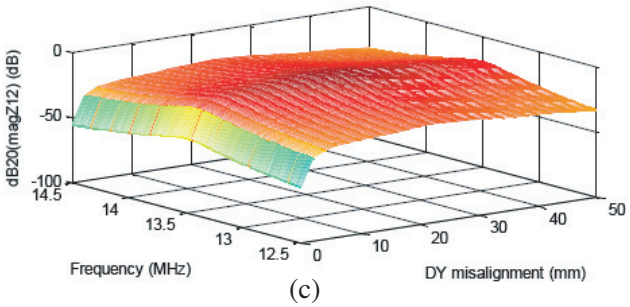

(c)

Figure 9. Level of simulated dB_{20} ($magZ_{12}$) versus the frequency band and the DY misalignment for $d = 10\,\text{mm}$ in VM mode. (a) A_{reader} in center. (b) B_{reader} in center. (c) E_{reader} in center.

The resonant frequency and bandwidth of the trans-impedance are affected by the lateral misalignment. However level of dB_{20} ($magZ_{12}$) seems more constant above the B_{reader} in comparison with the other DDC and less affected by the frequency variation. Higher value of dB_{20} ($magZ_{12}$), will allow the coupling to be more efficient, while a constant bandwidth frequency and negligible frequency shift will allow RFID data transfer. B_{reader} presents a better profile to enhance efficient and robust data transfer that confirms an improvement of RFID detection area.

Therefore, an array of overlapping small resonators would lead to efficiency in larger volume [22, 23]. In future studies several resonators will be inserted, and the distance between them could vary until their overlapping.

5. CONCLUSION

We have proposed an RFID system for detection of small tags using a reader coil in which a resonator is inserted, at its center. To improve the volume detection, an optimization has been realized to maximize the k_{eq}-factor by adjusting the diameter and turn number of the resonator sub-coils. The achievement of efficient tag detection performances has to be optimized in function of the coupling coefficient with the reader coil, its position on the surface of the coil and the Z-bandwidth of the equivalent trans-impedance. The proof-of-concept has been demonstrated though RFID detection measurements. Future works will focus on the insertion and overlapping of several DDC coils to maximize the detection volume. Additionally, the coupling coefficient between these DDC resonators and their detuning have to be evaluated and the impact on the detection depicted in order to optimize the energy transfer in a large dissipative volume. A methodology has to be found for this purpose and is currently being developed.

ACKNOWLEDGMENT

This research funded by Paris-Est University was conducted by M. Grzeskowiak over a six-months visiting period in Paris Electrical and Electronic Engineering Laboratory (GeePs) at Paris-Sud University.

REFERENCES

1. Zhang, R. and C.-H. Ho, "MIMO broadcasting for simultaneous wireless information and power transfer," *IEEE Transactions on Wireless Communications*, Vol. 12, No. 5, 1989–2001, 2013.
2. Mirbozorgi, S., H. Bahrami, M. Sawan, and B. Gosselin, "A smart cage with uniform wireless power distribution in 3D for enabling long-term experiments with freely moving animals," *IEEE Transactions on Biomedical Circuits and Systems*, Vol. 10, No. 2, 424–434, 2016.
3. Diet, A., C. Conessa, Y. Le Bihan, et al., "Detection tube for small HF RFID tags, based on mutual coupling with a coil resonator," *IEEE European Microwave Week (EuMC)*, 375–378, Sept. 2015.

4. Diet, A., C. Conessa, Y. Le Bihan, F. Alves, M. Grzeskowiak, M. Benamara, and G. Lissorgues, "LF RFID chequered loop antenna for pebble detection and area localization," *IEEE European Microwave Week (EMC)*, 41–44, Oct. 2016.
5. Zeng, Y., B. Clerckx, and R. Zhang, "Communicatios and signals design for wireless power transmission," *IEEE Transactions on Communications*, Vol. 65, No. 5, 2264–2290, 2017.
6. Bito, J., S. Jeong, and M. M. Tentzeris, "Heuristic passive and active matching circuit design method for wireless power transfer for moving objects," *Wireless Power Transfer (WPT)*, 1–4, May 2006.
7. Hwang, H., J. Moon, B. Lee, C. Jeong, and S. Kim, "An analysis of magnetic resonance coupling effects on wireless power transfer by coil inductance and placement," *IEEE Transactions on Consumer Electronics*, Vol. 60, No. 2, 203–209, 2014.
8. Fotopoulou, K. and B. W. Flynn, "Wireless power transfer in loosely coupled links: Coil misalignment model," *IEEE Transactions on Magnetics*, Vol. 47, No. 2, 416—430, 2011.
9. Mirbozorgi, S. A., P. Yeon, and M. Ghovanloo, "Robust wireless power transmission to mm-sized free-floating distributed implants," *IEEE Transactions on Biomedical Circuites and Systems*, Vol. 11, No. 3, 692–702, 2017.
10. Waters, B. H., B. J. Mahoney, G. Lee, and J. R. Smith, "Optimal coil size ratios for wireless power transfer applications," *IEEE International Symposium on Circuits and Systems (ISCAS)*, 2045–2048, Jun. 2014.
11. Shi, X. and J. R. Smith, "Large area wireless power via a planar array of coupled resonators," *IEEE International Workshop on Antenna Technology (iWAT)*, 200–203, Mar. 2016.
12. Choi, B. H., E. S. Lee, Y. H. Sohn, G. C. Jang, and C. T. Rim, "Six degrees of freedom mobile inductive power transfer by crossed dipole Tx and Rx coils," *IEEE Transactions on Power Electronics*, Vol. 31, No. 4, 3252–3272, 2016.
13. Kamineni, A., G.-A. Covic, and J.-T. Boys, "Analysis of coplanar intermediate coil structures in inductive power transfer systems," *IEEE Transactions on Consumer Electronics*, Vol. 30, No. 11, 6141–6154, 2015.
14. Sharma, A., I. J. Garcia Zuazola, A. Gupta, A. Perallos, and J. C. Batchelor, "Non-uniformly distributed-turns coil antenna for enhanced H-field in HF-RFID," *IEEE Antennas and Wireless Propagation Letters*, Vol. 61, No. 10, 4900–4907, 2013.
15. Benamara, M., M. Grzeskowiak, G. Lissorgues, A. Diet, Y. Le Bihan, and C. Conessa, "Calculation of the equivalent mutual impedance in complex HF RFID systems," *IEEE International Conference of Applied Electromagnetics and Communications (ICECOM)*, Sept. 2016.
16. Diet, A., M. Grzeskowiak, Y. Le Bihan, M. Biancheri-Astier, M. Lahrar, C. Conessa, M. Benamara, G. Lissorgues, and F. Alves, "Improvement of RFID HF tags detection with a distributed diameter coil," *IEEE Antennas and Wireless Propagation Letter*, Vol. 15, 1943–1946, 2016.
17. http://www.ansys.com/Products/Simulation+Technology/Electronics/Signal+Integrity/ANSYS+HFSS.
18. Finkerseller, A., *RFID Handbook*, Carl Hanser Verlag, Munchen, Germany, 2002.
19. http://www.nxp.com/products/identification-and-security/smart-labeland-tag-ics/icode:MC_4202.
20. sttID for 13.56 MHz Long Range Reader / Writer SIL-212. http://www.stt-rfid.com/node/101.
21. Diet, A., M. Biancheri-Astier, Y. Le Bihan, C. Conessa, F. Alves, M. Grzeskowiak, M. Benamara, and G. Lissorgues, "Design of 1 cm^2 coils for HF RFID instruments tracking with detection range improvement," *IEEE International Conference on RFID Technology & Application (RFID-TA)*, 2017.
22. Lee, H., S. Kang, Y. Kim, and C. Jung, "Small-sized metallic and transparent film resonators for MR-WPT system," *IEEE Electronics Letters*, Vol. 52, No. 8, 650–652, 2016.
23. Kang, S.-H., V.-T. Nguyen, and C.-W. Jung, "Analysis of MR-WPT using planar textile resonators for wearable applications," *IET Microwaves, Antennas and Propagation*, Vol. 10, No. 14, 1541–1546, 2016.